ELSEVIER

Journal of the Mechanics and Physics of Solids
52 (2004) 2101–2126

JOURNAL OF THE
MECHANICS AND
PHYSICS OF SOLIDS

www.elsevier.com/locate/jmps

Geometric and material nonlinearity during the deformation of micron-scale thin-film bilayers subject to thermal loading

Yanhang Zhang, Martin L. Dunn*

Department of Mechanical Engineering, University of Colorado at Boulder, Campus Box 427, Boulder, CO 80309-0427, USA

Received 12 September 2003; received in revised form 7 February 2004; accepted 9 February 2004

Abstract

We study, by experiments and modeling, the linear and geometric nonlinear behavior of thin-film bilayer mechanical structures subjected to thermal loading due to combined creep and stress relaxation. On the experimental side, we designed and fabricated a series of micron-scale gold (0.5 μm thick)/polysilicon(1.5 and 3.5 μm thick) beams and plates and initially thermal cycled them between room temperature and 190°C to stabilize the gold microstructure over this temperature range. After the initial thermal cycle, they are heated to 190°C where they are relatively flat, and then cooled to 120°C. During this temperature drop the thin film structures undergo linear and possibly geometrically nonlinear deformation depending on their size. They are then held at 120°C for about four weeks. During the thermal loading history we measured, using interferometry, full-field deformed shapes of the structures, from which curvature was determined. During the isothermal hold, creep and stress relaxation are observed in all of the structures, as manifested in significant curvature changes. We observe that both material and structural phenomena contribute to the observed deformation response. The interplay between the two is apparent in the plates where the initial cooling caused them to buckle, but the creep and stress relaxation then caused them to substantially unbuckle. We attempted to model the inelastic deformation by assuming simple power-law creep in the gold $\dot{\varepsilon} = A\sigma^n$, and assuming that the polysilicon did not relax at the modest temperature of 120°C. In order to accurately account for the dependence of curvature and stress on position, we carried out the calculations using the finite element method. We find that with such a simple model we can qualitatively describe all of the observed phenomena, however, some quantitative discrepancies exist. Finally, we carried out a parametric study of the effects of the structure shape and the power-law creep constants on the deformation, and studied the evolution of the stress state in the films both through the thickness and in the plane of the beams and plates. Regarding the stress state, initially a

*Corresponding author. Tel.: +1-303-492-6542; fax: +1-303-492-3498.
E-mail address: martin.dunn@colorado.edu (M.L. Dunn).

0022-5096/$ - see front matter
doi:10.1016/j.jmps.2004.02.003

significant stress gradient exists through the thickness of the films. Over time it becomes more uniform, and nearly constant in the creeping/relaxing metal film, but the gradient remains in the polysilicon film (that does not creep or relax).

Keywords: Thin film bilayer; Creep; Stress relaxation; Geometric nonlinearity; Microelectrochemical Systems (MEMS)

1. Introduction

Multilayer thin film material systems play a prominent role in numerous applications in microelectronics, optoelectronics, magnetic recording, and microelectromechanical systems (MEMS). An inherent characteristic of such systems is that misfit strains in the film layers lead to stresses in the layers and deformation of the structure upon a temperature change. A common source of misfit strains is differences in thermal expansion coefficients between the layers. For many applications, it is important to accurately control the deformation of thin film structures over a significant period of time in order to meet performance and reliability requirements. This is especially important for structures subjected to thermal loading and/or operated at elevated temperatures. When one or more of the layers consists of a metal or polymer film, the combined effects of creep and stress relaxation in the film can significantly influence deformation and compromise device performance, so these effects must be fully understood. Our work is motivated by applications in microelectromechanical systems (MEMS) where both short- and long-term dimensional stability are emerging as important issues for yield, performance, and reliability. For example, Miller et al. (2001) fabricated microrelay switch arrays for RF communications applications using prestressed gold/polysilicon bimaterial beams as electrostatically actuatable switches. They observed a change in the switch shape and position over time and attributed it to stress relaxation in the gold. Vickers-Kirby et al. (2001) report that creep in gold and nickel cantilever beams leads to voltage drops in micromachined tunneling accelerometers. These devices operate by applying a voltage to fix the position of the metal cantilever via electrostatic forces; a decrease in the voltage required means that less force is required to hold the cantilever in place. As will become apparent, creep and stress relaxation is especially interesting with MEMS-scale structures because the thin film layers are of comparable thicknesses. In this case the material nonlinearity, e.g., creep and stress relaxation, can interact with geometric nonlinearity, significantly complicating the resulting deformation behavior.

Creep and stress relaxation phenomena have been investigated in some detail for thin film on thick substrate systems, motivated primarily by microelectronics applications (see for example, Weiss et al., 2001; Keller et al., 1999; Shen and Suresh, 1995; Thouless et al., 1993, 1996; Thouless, 1995; Vinci et al., 1995; Flinn et al., 1987). These studies have focused on measuring, understanding, and modeling the stress vs. temperature behavior that occurs when a metal film/nonmetal substrate system is heated from room temperature, then cooled back to room temperature, over one or a few cycles. The stress–temperature curves in the experimental works were obtained using

the wafer curvature method, which is now widely used to measure stress in thin films. The method involves measuring the average curvature of a thick substrate covered by a thin film as a function of temperature change. During a typical test thermoelastic and inelastic mechanisms contribute to produce a complex nonlinear stress–temperature curve. Because the film is much thinner than the substrate, the stress in the film does not vary appreciably through its thickness. In addition, for small deformations, it is nearly constant over the planar dimensions of the film, varying appreciably from the average value only very near the edges. Finally, the stress state is typically equibiaxial plane stress. As a result, a single number is all that is required to quantify the *film stress*. Note that these comments refer to the stress as viewed at the scale of the film and substrate. In polycrystalline films microstructural-level stresses vary significantly at the grain and subgrain level depending on grain orientations and the level of anisotropy (Vinci et al., 1995; Baker et al., 2001; Spolenak et al., 2003). The beauty of the wafer curvature measurement technique is that because the deformation is controlled by the thick substrate, the film stress, regardless of its source, is easily computed from knowledge of the film/substrate curvature through use of the Stoney (1909) formula.

In most of the above-mentioned studies, the stress–temperature response is studied using wafer curvature measurements at a fixed heating or cooling rate so rate dependent and independent phenomena are coupled in the response. Stress relaxation during an isothermal hold has been studied by Hershkovitz et al. (1985), Doerner and Nix (1988), Flinn et al. (1987), Korhonen et al. (1990), Shute and Cohen (1992), Shen and Suresh (1995), Thouless (1995), Koike et al. (1998), and Keller et al. (1999). Thouless et al. (1993) measured stress relaxation of copper films on a silicon substrate at temperatures ranging from 74°C to 187°C. They found that the qualitative behavior was well-described by power law creep $\dot{\varepsilon} = A\sigma^n$, but argued that a mechanistic understanding of the values of A and n that were required was lacking. Shen and Suresh (1995) measured curvature evolution of thin aluminum film/silicon substrate systems during isothermal holds at 250°C that were imposed during both heating and cooling stages in cyclic thermal tests from room temperature to about 450°C. The stress relaxation process was most pronounced during the early stages of the isothermal hold. They attempted to model the phenomena using power-law creep in the aluminum and found that they could accurately describe the curvature evolution due to the stress relaxation with values of $A = 7 \times 10^{-18}$ and $n = 5.2$, where the units of $\dot{\varepsilon}$ and σ are s^{-1} and MPa, respectively. When a SiO_2 passivation layer covered the aluminum film, though, the predicted stress relaxation based on power-law creep in the aluminum far exceeded that observed experimentally, suggesting that the SiO_2 passivation alters the deformation properties of the aluminum film. Keller et al. (1999) studied isothermal stress relaxation of copper thin films on silicon substrates at temperatures between 40°C and 120°C. They were able to describe the relaxation data by power law creep of the copper with $n = 7$, but for good agreement they required a value of A that depended on film thickness. The reasons why this was necessary were not understood. Koike et al. (1998) studied stress relaxation of aluminum alloy films on silicon substrates at 100°C and 240^{c}C and interpreted the results to suggest three different deformation mechanisms occur over the temperature range of 300–650 K. The boundaries between the regions of different mechanisms were reasonably well described by a deformation

mechanism map modified to account for phenomena particular to thin films as suggested by Thouless et al. (1993). Consistent with Shen and Suresh (1995) they found that stress relaxation is most pronounced during the early stages of the isothermal hold.

These studies all show that significant stress relaxation can occur over periods of only a few hours at modest temperatures of only about 100°C for many metal thin film systems. Due to the thin film/thick substrate system, the stress in the metal films is quite high, on the order of hundreds of MPa. Models incorporating power law creep of the metal film were successfully able to describe the observed response qualitatively, and to a large degree quantitatively. However, the latter sometimes required modification of the power-law constants, presumably to account for differences in the microstructures of the films. The creep and stress relaxation were considered to be due to traditional mechanisms, but modified for the different constraint and stress state that exists in a thin film on a substrate.

In these studies, the films have been thermal cycled a few times so that the metal attains a state where the material microstructure is stable, and the creep and stress relaxation mechanisms result from traditional mechanisms. It is reasonably well known that metal films are often deposited in a state far from equilibrium and thus do not typically exhibit a stable microstructure in their as-deposited state. Exposing them to temperature excursions results in highly nonlinear deformation behavior during the first few cycles due to microstructural evolution such as annihilation of excess vacancies, void coalescence, and grain growth (Nix, 1989; Shen and Suresh, 1995; Koike et al., 1998; Baker et al., 2001; Legros et al., 2002). The microstructural evolution results in inelastic deformation, which at the continuum level can be treated as an inelastic strain, similar to plastic or creep strain (Zhang and Dunn, 2003). Quantitative models capable of predicting the evolution of the inelastic strain with loading (thermal and /or mechanical) over time in terms of the actual deformation mechanisms, though, are lacking. These phenomena are important in microsystems applications, though, because packaging processes will often subject the structure to modest temperatures between 100°C and 200°C where the inelastic deformation mechanisms are active.

In all of these studies the thin film structures consisted of a film on the order of 1 μm thick bonded to a substrate that was hundreds of μms thick. Much of the understanding gained regarding stress relaxation in these thin film/thick substrate systems, motivated strongly by microelectronics applications, is applicable to MEMS applications. Some significant differences exist, though, and these must be well understood to design high-yield, high-reliable MEMS. Perhaps the most significant difference is that in MEMS applications the layer thicknesses are not only small (on the order of μms) relative to in-plane dimensions, but they are often comparable. This can lead to much larger deflections, relative to the thickness of structures, than are observed in microelectronics applications, and make it necessary to include geometric nonlinearity in order to accurately model deformation. Furthermore, the geometric nonlinearity can lead to bifurcations in the deformation behavior for plate-like structures that possess high symmetry. These can be detrimental when dimensional stability is a requirement, or can be beneficial for actuator applications. Since the layers are of comparable thicknesses, stresses can vary appreciably through the thickness of the layers, unlike in microelectronics applications where the stress is essentially uniform in the film. The stresses

are also typically smaller as they are relaxed substantially by curvature. In addition, the curvature, and thus stresses, can vary significantly over the in-plane dimensions of the structure (Finot and Suresh, 1996; Finot et al., 1997; Freund et al., 1999; Freund, 2000; Lee et al., 2001; Dunn et al., 2002). A number of studies have elucidated the basic thermomechanical response of thin film/substrate systems in the geometrically nonlinear regime (Fahnline et al., 1991; Masters and Salamon, 1993; Salamon and Masters, 1995; Finot and Suresh, 1996; Finot et al., 1997; Freund et al., 1999; Freund, 2000; Lee et al., 2001) and the reader is referred to these for details. Although the early motivation for the study of this phenomena was to predict the shape of structural composite laminates after elevated temperature curing (Hyer, 1981a, b, 1982), more recent technological motivation comes from the continued development by the microelectronics industry of thinner, but larger diameter, silicon wafers, approaching 50 μm thick and 300 mm diameter (Laduzinsky, 2001). In MEMS applications geometrically nonlinear phenomena can also occur because even though the in-plane dimensions are small, for example, a few hundred μm, the thicknesses are on the order of only 1 μm. This is easily seen from Freund's (2000) nondimensional criterion for the existence of geometric nonlinearity. We have previously observed and studied these geometrically nonlinear phenomena for thin film gold/polysilicon plates subjected to thermal loading (Dunn et al., 2002).

In this work, we consider the interesting interaction between the geometrically nonlinear structural response and creep and stress relaxation during uniform thermal loading for thin-film beams and plates. We use the terms creep and stress relaxation a bit loosely to refer to the time-dependent inelastic deformation that is observed. This includes the effects of traditional mechanisms, and also the effects of microstructural evolution such as recovery, recystallization, and grain growth. We study these effects both by experiments and modeling, using experimental observations to guide the scope of the modeling efforts. To this end we begin by describing the design and fabrication of the thin-film structures and our measurement methods. We follow this with measurement results that illustrate the basic phenomena, and then we describe our efforts to model these phenomena. Complete measurement and modeling results are then presented and discussed in detail, followed by a summary of conclusions. We emphasize that while we focus on thin-film structures consisting of beam- and plate-like gold/polysilicon bilayers, the general results are much more broadly applicable.

2. Samples and measurements

We designed a series of thin film structures in the form of both beams and square plates. We use the term *beam* for convenience, recognizing that even for the planar aspect ratio of the structures, plate theory, rather than beam theory, is formally required to describe the deformation. Nevertheless, we will refer to these structures as *beams* to conveniently discriminate between the square plates which we will refer to as *plates*. The thin film structures consist of a 0.5 μm thick gold film that fully covers either a 1.5 μm or 3.5 μm thick polycrystalline silicon (polysilicon) film. Square plates of sizes $L \times L$ were fabricated with $L = 200$ and 300 μm. Beams 280 μm long $\times 50$ μm

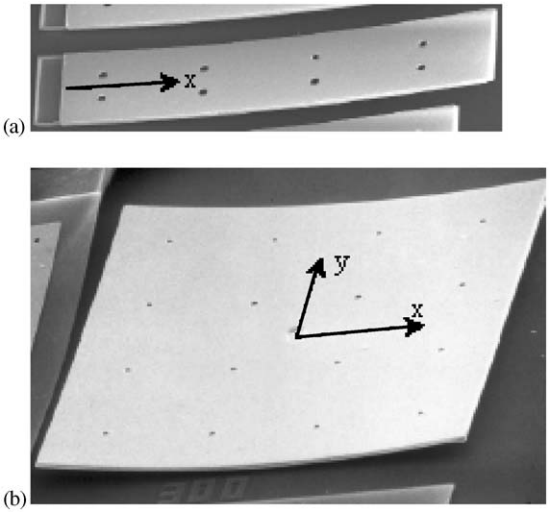

Fig. 1. Scanning electron micrograph of gold (0.5 μm thick)/polysilicon (1.5 μm thick) structures. The support post and etch holes are apparent and the x–y coordinate system used in subsequent measurements and analysis is identified: (a) 280 μm × 50 μm cantilever beam; (b) 300 μm × 300 μm square plate.

wide were fabricated. The idea behind the design is to yield gold/polysilicon bilayer structures that are attached to the substrate in a manner that minimizes the effect of the attachment since structures this size will adhere to the substrate if they are not supported above it in some manner. To this end, the plates were attached to the substrate by a 16 μm diameter polysilicon post at the center, and the beams were cantilevered from the substrate by a 16 μm × 46 μm polysilicon support, as is evident in Fig. 1.

The gold/polysilicon beams and plates were fabricated using the commercially available Multi-User MEMS Process (MUMPs, Koester et al., 2001). The so-called surface micromachining process consists of a series of standard microelectronics lithography, thin-film deposition, and etching processes. Briefly, the relevant steps of the complete process consist of depositing a 2 μm thick sacrificial film of phosphosilicate glass (PSG) on top of a 600 nm thick silicon nitride film on a (1 0 0) single crystal silicon wafer by low pressure chemical vapor deposition. A 2 μm thick polysilicon film (Poly 1) is then deposited on the PSG, patterned, and etched. A second PSG film, 200 nm thick, is then deposited and the wafer is annealed to dope the polysilicon with phosphorus from both PSG films, and to reduce the residual stress in the polysilicon film. The top PSG and polysilicon films are lithographically patterned and etched to produce the desired beam and plate shapes and sizes. Another 0.75 μm thick PSG film is then deposited, followed by a second 1.5 μm thick polysilicon film (Poly 2), and another 200 nm PSG film to serve as a mask for patterning and etching the Poly 2 layer to conform to the desired beam and plate shapes and sizes. This is followed by another annealing process to minimize residual stresses and stress gradients. A 99.999%, 0.5 μm gold film is then e-beam evaporated over a 20 nm thick chromium adhesion layer, and then lift-off patterned. Finally, the structures are freed from the substrate by etching

away the PSG film in a 49% hydrofluoric acid solution. In order to assure the etchant attacks the PSG completely and in a timely manner, etch holes are patterned in the structures to provide an easy flow path for the etchant. Scanning electron micrographs of typical beams and plates are shown in Fig. 1.

Full-field measurements of the out-of-plane displacement of the structures were made as a function of temperature change with scanning white light interferometry using an interferometric microscope and a custom-built temperature chamber. The resolution of the out-of-plane displacement measurements, $w(x, y)$, is at least 5 nm as verified by making measurements on standards, and the resolution of the temperature chamber is about 1°C. During tests a Michelson objective was used which has a beam-splitting element that transmits one portion of the white light beam to a reference mirror and the other to the object. The two beams reflected from the reference and the object are recombined and projected onto a charge-coupled device (CCD) video camera to generate a signal proportional to the resultant beam intensity produced by the interference effect. These signals are then transferred into the spatial frequency domain and the surface height for each point is obtained from the complex phase as a function of the frequency. Complete details of the data reduction algorithm are given by De Groot and Deck (1995) where they report subpixel/fringe accuracy of 0.1 nm (De Groot and Deck, 1995). We do not claim to have achieved such accuracy, but in our measurements we are confident that we achieve nm-scale accuracy that is more than sufficient for our purposes. We used a 5X Michelson objective to yield a lateral spatial resolution of about 2.7 μm.

The primary objective of the experimental program was to measure deformed shapes of the structures as a function of temperature during cooling and then time at elevated temperature holds in order to study the effects of creep and stress relaxation. To this end, each test proceeds as follows. First, the structures are thermal cycled three times between room temperature and 190°C to try to stabilize the gold microstructure since it is well-known that significant microstructural evolution can occur during the first thermal cycle after deposition (see, for example, Nix, 1989; Leung et al., 2000; Thouless et al., 1993, 1996; Shen and Suresh, 1995; Koike et al., 1998; Keller et al., 1999; Baker et al., 2001; Weiss et al., 2001). During this process the temperature is held constant for $\approx$ 3.5 min roughly every 15°C so that thermal equilibrium is reached. After the initial thermal cycles, the structures are cooled from 190°C to 120°C at a rate of 10°C/min. At 190°C the structures are nearly flat. The deformation during the cooling to 120°C is then due primarily to linear and geometrically nonlinear thermoelasticity. The structures are then held at 120°C for about 4 weeks ($\approx$ 700 h). We measured full-field out-of-plane displacements as a function of temperature during the initial thermal cycles, the subsequent temperature drop from 190°C to 120°C, and as a function of time during the isothermal hold at 120°C. Two sets of experiments, referred to as experiment 1 and 2 throughout the paper, were carried out, in which the rate of heating and cooling was the same.

From the measured $w(x, y)$, we calculate the curvatures $\kappa_x(x, y) \approx -\partial^2 w/\partial x^2$ and $\kappa_y(x, y) \approx -\partial^2 w/\partial y^2$ over a region of about 150 μm. For the plates the measurement region is about 150 μm diameter around the center of each plate, while for the beams the region is of 150 μm length adjacent to the cantilever support. We measure only

over this region, and not over the entire plate, because the slope of the displacement field outside this region is too large to be measured with the 5X objective. The average curvatures over these regions are determined by fitting $w(x, y)$ with a sixth-order polynomial along $x=0$ and $y=0$, and then differentiating and averaging as appropriate. For the most part we characterize the deformation in terms of the average curvature, although we recognize that substantial nonuniformity can exist during nonlinear deformation (see, for example, Freund et al. (1999), Freund (2000), and Finot et al. (1997) for theoretical studies and Finot et al. (1997), Dunn et al. (2002), and Lee et al. (2001) for experimental studies).

3. Observations: basic phenomena

Fig. 2 shows the average curvature as a function of temperature between 190°C and room temperature for a gold (0.5 μm thick)/polysilicon (3.5 μm thick) 280 μm × 50 μm beam during the first three thermal cycles between room temperature and 190°C. For the beams, the curvature was found not to vary with position except within a localized area close to the support post, and thus the deformation is well-described by the average curvature. The response shows three regimes of deformation:

(i) During the initial heating the deformation is thermoelastic, characterized by a decrease in curvature with a constant $d\kappa/dT$, until the temperature reaches about 75°C.

(ii) Between 75°C and 190°C, the curvature changes at a much smaller rate; in fact $d\kappa/dT \approx 0$. This suggests that significant temperature-induced microstructural changes occur in the gold film during the first thermal cycle which result in tensile straining of the film. These compete with the thermoelastic deformation, resulting in $d\kappa/dT$ being much smaller than the thermoelastic value.

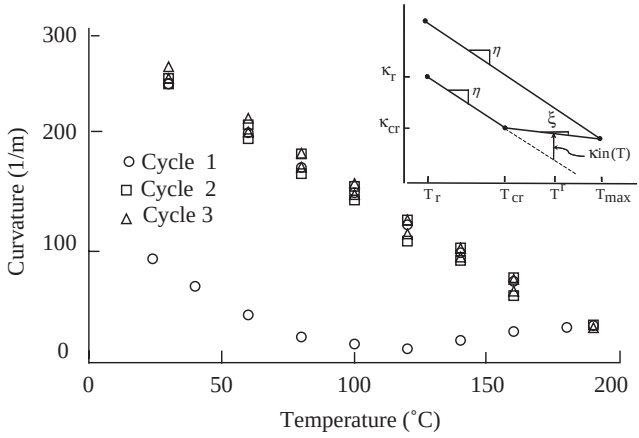

Fig. 2. Measured curvature during thermal cycling between room temperature and 190°C before the isothermal tests for gold (0.5 μm thick)/polysilicon (3.5 μm thick) 280 μm × 50 μm beam. The inset shows parameters describing the idealized response of the beam.

(iii) Upon cooling from 190°C, the response is again thermoelastic throughout the entire cooling process. If the structures were cooled below room temperature or if they were heated to a higher temperature and then cooled, plastic deformation could occur during cooling. The curvature upon return to room temperature is larger than that initially at room temperature.

Typical mechanisms that have been reported in the second deformation regime include densification, defect annihilation, and grain growth (see for example, Nix, 1989; Shen and Suresh, 1995; Koike et al., 1998; Leung et al., 2000; Baker et al., 2001), although the latter seems unlikely at such low temperatures (the melting temperature of gold is about 1337 K). Using high-resolution scanning electron microscopy we have studied the evolution of the gold microstructure during this first cycle. Upon release, the gold microstructure consists of a fine, roughly columnar, grain structure (average grain size about 500 nm). Upon heating to 200°C and cooling, scanning electron microscopy of the surface suggests coalescence of the subgrain structure, but no significant growth of the overall grains. Preliminary transmission electron microscopy, though, does show some grain growth. The film is likely undergoing a recovery process analogous to annealed bulk solids where defects are annihilated at temperatures below the recrystallization temperature. This would result in tensile straining of the gold film, consistent with the observed curvature response, although the magnitude of this effect is difficult to quantify. Heating to higher temperatures, say 500–600°C, and holding for longer times leads to observable grain growth, but associated with this is a loss of reflectivity of the gold so we do not study the behavior at these elevated temperatures. After the first cycle the material microstructure appears to be stabilized, at least over this temperature range and time period. Even though there is a slight amount of hysteresis upon heating and cooling, it is far less than that which occurs during the first cycle. Other beams and plates exhibit similar behavior, except the magnitude of the curvature differs accordingly. In addition, the plates exhibit nonlinear response upon cooling, a feature we will discuss later.

Fig. 3(a) shows the average curvature in the x- and y-directions vs. temperature during the cooling process from 190°C to 120°C for $L=200$ and 300 μm gold (0.5 μm thick)/polysilicon (1.5 μm thick) plates. Here and throughout we will take κ_x to be the larger, and κ_y the smaller, of the two principal curvatures if they are not equal. If they are equal we will just use $\kappa = \kappa_x = \kappa_y$ to denote the curvature. As has been previously shown both theoretically and experimentally (Hyer, 1981a, b, 1982; Finot and Suresh, 1996; Finot et al., 1997; Freund, 2000; Freund et al., 1999; Masters and Salamon, 1993, 1994; Dunn et al., 2002), the deformation during the temperature drop generally includes three regimes: (i) linear thermoelastic response independent of plate size, (ii) geometrically nonlinear thermoelastic response that depends on plate size, and (iii) bifurcations in the curvature–temperature response that also depend on plate size. All three of these regimes are observed in the response in Fig. 3, as is the plate size dependence; the $L = 300$ μm square plate has bifurcated and deformed into a nonsymmetric shape at $T = 120$°C, while the $L = 200$ μm plate has not. Although the sparseness of our data does not conclusively demonstrate the first regime of linear thermoelastic behavior independent of plate size, previous more detailed studies in this

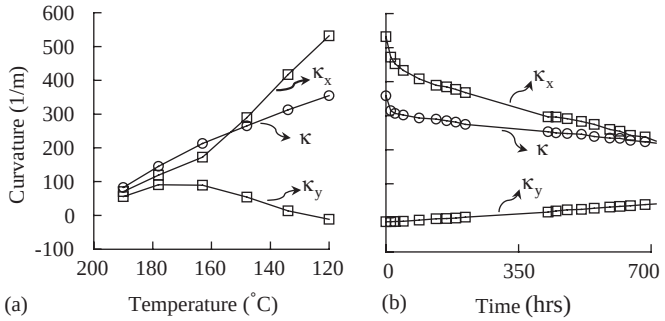

Fig. 3. (a) Curvature vs. temperature during cooling from 190°C to 120°C and (b) curvature vs. time during the isothermal hold at $T = 120°C$ for gold (0.5 μm thick)/polysilicon (1.5 μm thick) $L \times L$ square plates; $L = 200$ μm (circles) and $L = 300$ μm (squares). The measured data are connected by lines to aid viewing.

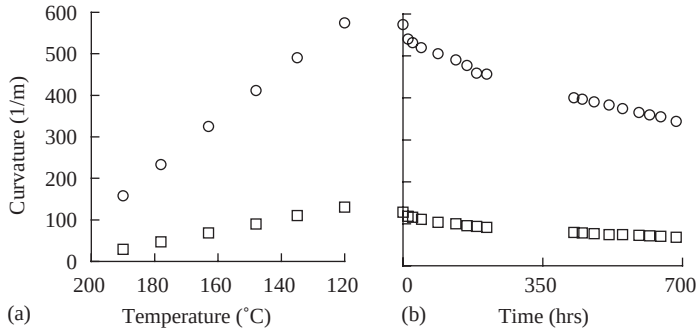

Fig. 4. (a) Curvature vs. the temperature during cooling from 190°C to 120°C and (b) curvature vs. time during the isothermal hold at $T = 120°C$ for 280 μm × 50 μm gold (0.5 μm thick)/polysilicon (1.5 μm thick) (circles) and gold (0.5 μm thick)/polysilicon (3.5 μm thick) (squares) beams.

regime do (Dunn et al., 2002). When the temperature change becomes large enough to cause geometric nonlinear behavior, the curvature of the $L = 300$ μm plate is less than that of the $L = 200$ μm plate except at temperatures below about 150°C where κ_x exceeds the curvature for the $L = 200$ μm plate. This is consistent with our previous modeling results (Dunn et al., 2002).

Fig. 4(a) shows the curvature along the long axis of the beam κ_x vs. temperature during the cooling process for a 280×50 μm gold (0.5 μm thick)/polysilicon (1.5 μm and 3.5 μm thick) beam. While three deformation regimes are apparent for the plates, only a single one appears for beams: linear thermoelastic response. Although not shown, measurements for other beam lengths show that the curvature is independent of beam length as expected. This is because it is more energetically favorable for the beams to approach a state of cylindrical bending, as this deformation mode can be accomplished without straining of the midplane (in excess of the strain that occurs due to the bi-material effect). The slope of the curvature vs. temperature curve is about four times

greater for the structure with 1.5 μm thick polysilicon films than that for the 3.5 μm thick films.

During the isothermal hold, the combined effects of creep and stress relaxation are clearly observed in all of the structures as manifested in a decrease in curvature. Formally, we refer to both creep and stress relaxation because neither the stress nor strain remains constant during the isothermal hold. Representative measurements are shown in Figs. 3(b) and 4(b), for plates and beams, respectively. Qualitatively the behavior is similar for the $L = 200$ μm plate and the beams; the curvature decreases significantly over the isothermal hold period. The rate of decrease of the curvature is rapid over the first 48 h, then remains roughly constant. The behavior of the $L = 300$ μm plate which bifurcated upon cooling is different and quite interesting. The principal curvature κ_x decrease monotonically in a manner similar to $\kappa = \kappa_x = \kappa_y$ for the $L = 200$ μm plate. The curvature κ_y, however, *increases* with time. Over time both κ_x and κ_y evolve significantly from their values at $t = 0$. Again the rate of change of curvature decreases after about 48 h and then does not change significantly over the rest of the holding time. In summary, the $L = 300$ μm plate exhibits the interesting phenomena that it *buckles* during the cooling due to geometric nonlinearity, then tends to *unbuckle* during the isothermal hold due to material nonlinearity.

4. Analysis

Our aim is to model the phenomena observed in the previous section in as simple a manner as possible, and then identify possible shortcomings in the model that can be studied later. It is not to develop a mechanism-based model of the inelastic behavior of the film. Formally, this effort requires modeling the deformation during the first cycle, during heating to 190°C, during cooling to 120°C, and then during the isothermal hold. Modeling of the phenomena during the first cycle is particularly difficult because the constitutive response of the gold film is complex and unknown. We recently proposed a simple model for bilayers that requires four parameters as shown in the inset of Fig. 2 (Zhang and Dunn, 2003). We do not follow this line of inquiry further in this work, but instead, we recognize that the stresses in the films are small at the elevated temperature, at least when compared to those developed upon cooling. For simplicity, we then assume that the stresses are zero at the beginning of cooling, and model the stress and curvature development upon cooling and during the isothermal hold.

We used the Abaqus finite element code with four-node composite plate elements that approximate the thin-plate kinematics of the Kirchhoff theory. Geometric nonlinearity is modeled using the well-known von Karman theory for thin plates with large deflections. Both materials are modeled as linear elastic with isotropic material properties. Input parameters to the finite element calculations are $E_2 = 163$ GPa, $\nu_2 = 0.22$ (Sharpe, 2002), $E_1 = 78$ GPa, $\nu_1 = 0.42$ (King, 1988). Here and throughout we take subscripts 1 and 2 to denote properties associated with the gold and polysilicon, respectively. The thermal expansion coefficients of the materials were assumed to vary linearly with temperature and values at 190(120)°C are $\alpha_2 = 3.5(3.2) \times 10^{-6}/°C$, and $\alpha_1 = 15.1(14.6) \times 10^{-6}/°C$ (King, 1988). Although some uncertainty exists in the values

of these material properties for the gold and polysilicon films, we think that they are accurate enough for the purpose of modeling the observed phenomena. Young's modulus and Poisson's ratio of the polysilicon are in line with many measurements over many MUMPS runs (Sharpe, 2002), and agree adequately with bulk polycrystal averages of single crystal elastic constants. Although we used temperature-dependent properties in the calculations, if the properties are assumed not to vary with temperature, the effect is insignificant for the materials and temperature range considered here.

Calculations were carried out for the loading situation of an applied uniform temperature change from the temperature at which the curvature is zero (inferred from the experiments by extrapolation of the measurements from 190°C to 120°C). The zero-curvature temperature obtained in this manner varies slightly for the different structures, averaging 205°C with a standard deviation of 5°C for the samples with 1.5 μm thick polysilicon, and 213°C with a standard deviation of 1°C for the samples with 3.5 μm thick polysilicon. We assume the stress in the films is zero at zero curvature. The adequacy of this assumption will be discussed later when we discuss the operative deformation mechanisms in the gold film.

Typical finite element meshes for the plates contained elements with a characteristic dimension of about 12.5 μm, a size that was chosen after a convergence study with mesh size. Calculations incorporating the support post showed that it had insignificant effects on the resulting displacements, curvatures, and stresses except in a region very near the post. If one carries out calculations as just described, the linear and geometrically nonlinear response of the plate can be computed, but the bifurcations, and the subsequent post-bifurcation behavior, cannot because of the perfect symmetry present in the geometry and material behavior. A reasonable way to model the bifurcations is to seed an imperfection of some sort into the model. There are a number of possible actual imperfections that can trigger the bifurcation, including slight differences in the plate lengths in the x- and y-directions, slight variations in the plate thickness, and slight anisotropy in the thermoelastic moduli of the materials. It turns out that slight thermal expansion anisotropy gives rise to behavior in the gradual bifurcation and post-bifurcation regimes, e.g., between 160°C and 120°C very much like that in Fig. 3. In light of this observation, we introduced slight anisotropy into the model by assuming the thermal expansion coefficient of the gold is orthotropic. Specifically, we defined the in-plane thermal expansion coefficients to be $\alpha_x = \alpha_1$ and $\alpha_y = \alpha_1 + \delta\alpha_1$, where $\delta\alpha_1$ was nominally taken to be 0.01% of α_1. As described by Dunn et al. (2002), the thermal expansion of gold, even a highly textured film, would not be expected to be orthotropic since gold single crystals are cubic. Nevertheless, the combined effects of thermal expansion and elastic properties are really of importance, as opposed to each individually, and a slight anisotropy of this magnitude is a fair amount less than the resolution of current methods to measure thin-film thermoelastic properties and is probably not unreasonable. With this slight perturbation, the pre-bifurcation response was indistinguishable from that with the isotropic thermal expansion. As discussed by Freund (2000), though, details of the bifurcation, especially its sharpness, are strongly influenced by small changes in the imperfection.

The second step of the calculations is the stress relaxation during the isothermal hold. The starting point for these calculations is the ending point of the first step. We modeled

the stress relaxation process by assuming simple power-law creep in the gold, $\dot{\varepsilon} = A\sigma^n$, and assuming the polysilicon deformed elastically at the modest temperature of 120°C. Within Abaqus, the power-law creep is implemented in a standard multiaxial formalism through the Mises stress potential. Accurate values of the power law parameters are not available for the gold films so we studied their influence over a reasonable range and then tried to assess their values by fitting model results to the experiment data for the beams. With this simple approach, the values of A and n are meant to incorporate any effects of the thin (20 nm) chromium adhesion layer which has an insignificant effect on the thermoelastic behavior. In order to provide reasonable initial conditions for the simulation of the deformation during the isothermal hold for the case of the bifurcated plate, we take advantage of the observation that the details of the bifurcation are extremely sensitive to imperfections. Specifically, we adjusted the thermal expansion anisotropy in the gold film so that the predicted κ_x and κ_y matched the measurements at $T = 120$°C, $t = 0$ h. We note that this results in no significant effect in the predicted pre-bifurcation behavior.

5. Results and discussion

The results of Figs. 3 and 4 in terms of the average curvature suffice to largely portray the overall deformation behavior. More detail regarding the deformation during the isothermal hold is presented in Fig. 5 where contour plots showing full-field deformed shapes of beams and plates are shown at four times: $t = 0$, 160, 428, and 684 h. Fig. 5a shows results for the 280×50 μm beam and Figs. 5b and c show results for the $L = 200$ μm and 300 μm plates, respectively. For all three cases, both measurements and predictions are shown. The deformation of the beams as a function of time shows the evolution of curvature as the number of contours decreases. The predictions are in good agreement with the measurements; both are able to pick up the slight variation of curvature across the beam. The circular contours of Fig. 5(b) show that the $L = 200$ μm plate deforms symmetrically at the beginning, and continues to deform symmetrically throughout the isothermal hold. As with the beams, during the isothermal hold the number of contours decreases, which indicates that the deflection and curvature decreases, presumably due to creep and stress relaxation in the gold. The measured behavior is also accurately described by the predictions. Fig. 5c shows that the $L = 300$ μm plate, which has buckled during the thermoelastic deformation, tends to unbuckle during the isothermal hold. At the beginning of the isothermal hold the plate is buckled as seen by the ellipsoidal displacement contours. During the isothermal hold, not only does the number of displacement contours decrease, but the shape of the displacement contours changes, becoming less ellipsoidal, illustrating that the plate has unbuckled to some degree. This is the same phenomena as seen in Fig. 4(b) in terms of the average curvature in the x- and y-directions during stress relaxation. Again the predictions are in good agreement with the measurements. We note though that because of the large slope of the deflections at $t = 0$ we can only measure part of the entire plate and this is the region shown in the contours. As the plate flattens with time, a larger region of the plate becomes experimentally accessible.

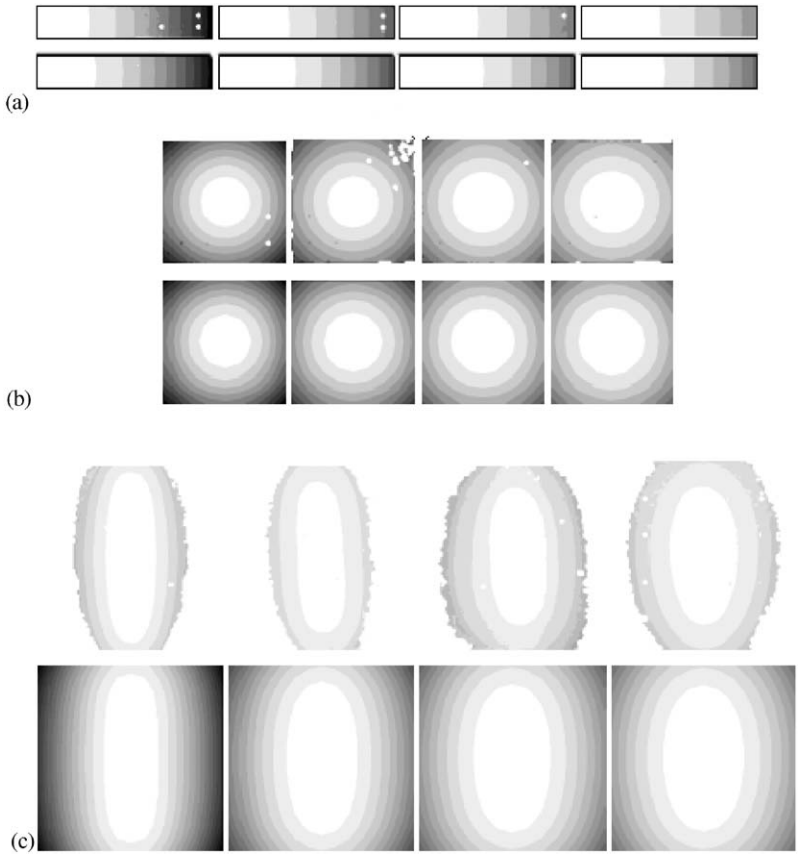

Fig. 5. Measured (top) and predicted (bottom) full-field displacement contours over a entire gold/polysilicon structure during the stress relaxation process: (a) gold (0.5 μm thick)/polysilicon (3.5 μm thick) 280 μm × 50 μm beam, each contour represents 0.6 μm; (b) gold (0.5 μm thick)/polysilicon (3.5 μm thick) 200 μm × 200 μm plate, each contour represents 0.12 μm; and (c) gold (0.5 μm thick)/polysilicon (1.5 μm thick) 300 μm × 300 μm plate, each contour represents 0.67 μm. Plots in (a) and (b) and (c) correspond to $t = 0$, 160, 428, and 684 h, respectively, from left to right. The beams are cantilevered from the left end, and the plates are supported at the center.

Fig. 6 shows the measured and predicted curvature development during the isothermal hold at 120°C for gold (0.5 μm thick)/polysilicon (3.5 μm thick) 280 μm × 50 μm beams. The circles and squares represent data for two different, but nominally identical, beams. With $n = 5$ and $A = 9 \times 10^{-16}$ h^{-1} MPa^{-5}, the deformation behavior over a time period of about 700 h (4 weeks) is well described. While these parameters were chosen to fit the data, they are in reasonable agreement with thin film data in the literature as described earlier, particularly, the power-law exponent. During the isothermal hold, creep and stress relaxation occur in the gold film and this is manifested as a decrease in curvature of the structure. Over the hold period of 700 h, the curvature of the beams

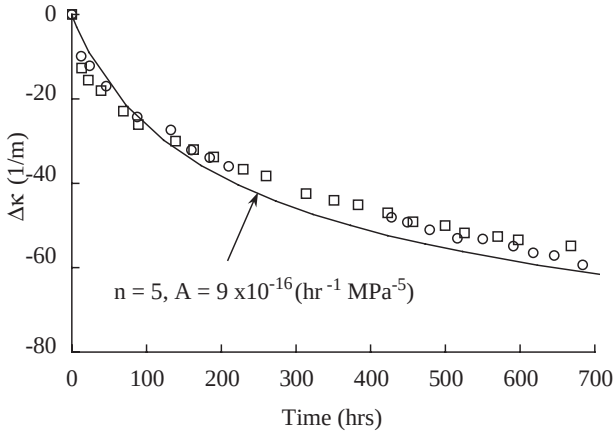

Fig. 6. Curvature change during the isothermal hold at 120°C of 280 μm × 50 μm gold (0.5 μm thick)/polysilicon (3.5 μm thick) beams. The circles and squares are measurements; the solid line is a calculation using power-law creep in the gold.

decreases by about 60 m^{-1} which is about 43% of the initial curvature. The two beams from the two experiments do not show significant differences.

In Fig. 7 we show corresponding results for $L = 200$ and 300 μm plates of the same thickness (0.5 μm thick gold and 3.5 μm thick polysilicon) as the beams in Fig. 6. Note that the $L = 300$ μm plate does not bifurcate like that in Fig. 3 because of the increased polysilicon thickness. These results for the two polysilicon thicknesses (1.5 μm in Fig. 3 and 3.5 μm in Fig. 7) illustrate the sensitivity to geometry (in the range of practical thin-film structures) on the structural behavior. The calculations are done using the n and A determined from the fit to the data for beams in Fig. 6, and agree well with the measurements over the duration of the isothermal hold.

In Figs. 8–10 we show companion results for the beams and plates with a 0.5 μm thick gold film and a 1.5 μm thick polysilicon film. Fig. 8 shows the curvature during the isothermal hold for 280 μm × 50 μm beams. Compared to the results in Fig. 6 the curvature at $t = 0$ is about four times higher due to the decreased polysilicon film thickness. This dependence is well described by the thermoelastic analysis. We attempted to use the same values of n and A to predict the curvature evolution during the isothermal hold of these structures, and the results are shown by the dashed line in Fig. 8. Clearly, the predictions do not agree well with the measurements as they significantly underestimate the decrease in curvature due to the effects of the creep and stress relaxation. The reasons for this are not completely clear, but the results resonate with similar studies of thin films on thick substrates in microelectronics contexts. For example, in their simulations of stress relaxation of metal films on thick substrates, Keller et al. (1999) found that to obtain good agreement between predictions and measurements they could use a constant power-law exponent n, but they had to use a thickness-dependent activation energy and temperature-dependent dislocation density. This corresponds to using a thickness dependent A in our simulations, however, there

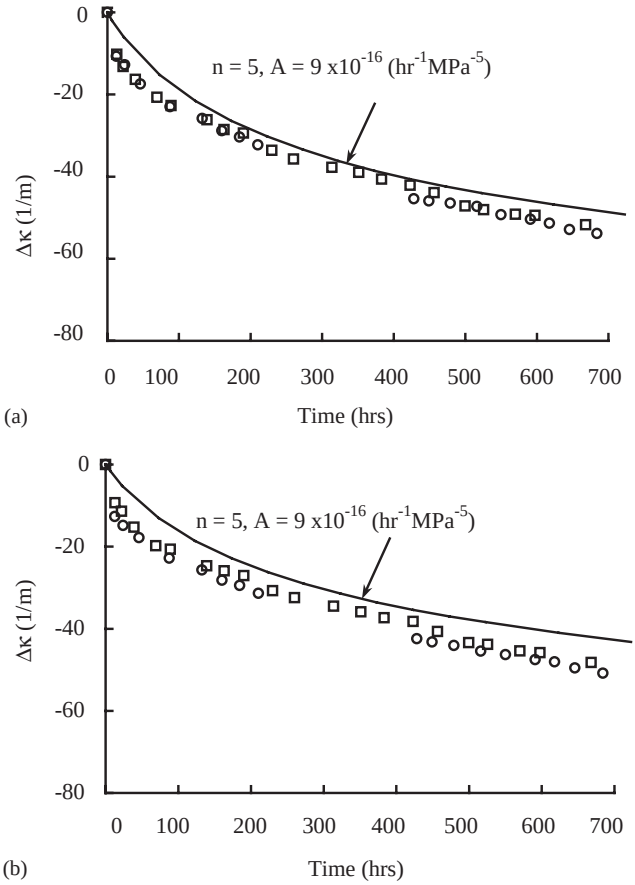

Fig. 7. Curvature change during the isothermal hold at 120°C of (a) 200 μm × 200 μm; and (b) 300 μm × 300 μm gold (0.5 μm thick)/polysilicon (3.5 μm thick) plates. The circles and squares are measurements; the solid line is a calculation using power-law creep in the gold.

are differences. In their study the metal film thickness was varied while the *thick* substrate thickness was unchanged. In our study, the metal film thickness is kept the same while the *thin* substrate thickness is varied. Unlike their situation with a thick substrate relative to the film, in our samples there are substantial stress variations through the thickness of the layers since they are of comparable thickness. The stress gradient in the 0.5 μm thick gold/1.5 μm thick polysilicon film is higher than that in the 0.5 μm thick gold/3.5 μm thick polysilicon film, although the magnitude of the stress is less (this will be discussed in some detail later). In the calculations, if we keep $n = 5$, but increase A to 5.2×10^{-15} h^{-1} MPa^{-5}, we get reasonable agreement between the predictions and measurements, the latter being the solid line in Fig. 8. After 700 h, the curvature has decreased by 200–300 m^{-1}, about 50% of the initial curvature.

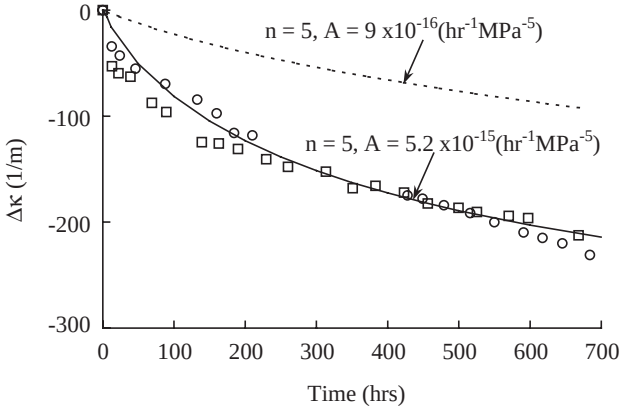

Fig. 8. Curvature change during the isothermal hold at 120°C of 280 μm × 50 μm gold (0.5 μm thick)/polysilicon (1.5 μm thick) beams. The circles and squares are measurements; the lines are calculations using power-law creep for the gold.

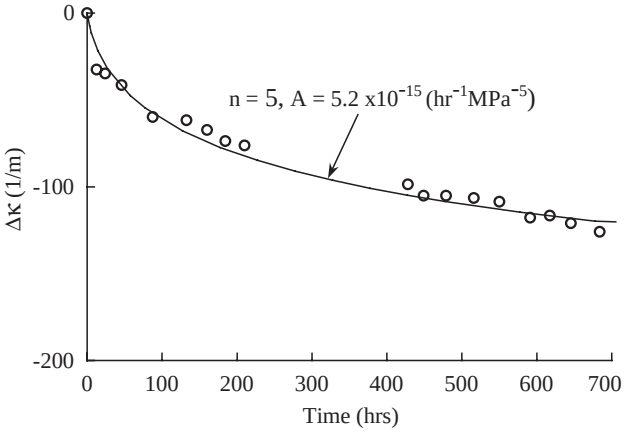

Fig. 9. Curvature change during the isothermal hold at 120°C of 200 μm × 200 μm gold (0.5 μm thick)/polysilicon (1.5 μm thick) plates. The circles are measurements; the solid line is a calculation using power-law creep in the gold.

A likely source of the discrepancy between the predictions and the measurements for different polysilicon film thicknesses is the inadequacy of the simple power-law creep model for the deformation of the gold film. Recent studies on similar gold/polysilicon beams (Gall et al., 2004) suggest that in addition to the creep/stress-relaxation mechanism, a recovery mechanism, likely resulting from microstructural changes, occurs. This mechanism results in compressive straining of the gold film, and it probably is necessary to include it in the constitutive model of the gold to obtain quantitative agreement for the deformation as a function of stress state (polysilicon thickness). Furthermore,

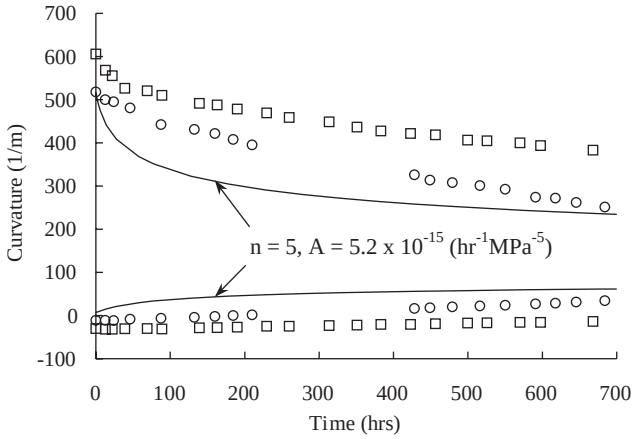

Fig. 10. Curvature during the isothermal hold at 120°C of 300 μm × 300 μm gold (0.5 μm thick)/polysilicon (1.5 μm thick) plates. The circles and squares are measurements; the solid lines are calculations using power-law creep in the gold.

it is possible that the stress states in the gold films, although different by less than a factor of two, are sufficiently different so as to result in a different deformation mechanism being operative in each case. While this is somewhat speculative, its plausibility is supported by the recent work of Huang (1998) who constructed a deformation mechanism map for fcc copper thin films. The normalized stress–temperature combinations of our work appear to lie very near the power law creep boundary on the deformation mechanism map. This suggests that our samples could be close to the boundary separating different deformation mechanisms. In Figs. 9 and 10 we compare measurements and predictions of the relaxation behavior of the plates with 1.5 μm polysilicon films, using $n = 5$ and $A = 5.2 \times 10^{-15}$ h^{-1} MPa^{-5}, since it adequately describes the behavior of beams in Fig. 8. Fig. 9 shows the measured and predicted results for the $L = 200$ μm plate. As shown in Fig. 3, the deformation of this structure is symmetric, i.e., there is no bifurcation. The prediction agrees well with the measurements. Fig. 10 shows corresponding measurements and predictions for the $L = 300$ μm plates. At the initial point of the stress relaxation process, the structure is deformed into an ellipsoidal mode, i.e., $\kappa_x \neq \kappa_y$, as shown in Fig. 3 and the first plot of Fig. 5c. The measurements show that during the isothermal hold, the curvature κ_x decreases while κ_y increases, and the rate of decrease of κ_x is greater than the rate of increase of κ_y. Over time both κ_x and κ_y evolve significantly from their values at $t = 0$, indicating that the plate is trying to unbuckle from an ellipsoidal mode to a circular mode. The measurements are from two nominally identical samples, but processed in different fabrication runs. The results agree qualitatively, however there is some quantitative variability between the two sets of data. This variability is larger than that in the cases where there is no bifurcation. This is consistent with pure thermoelastic deformation where there is significantly more variability in the details of the bifurcation than in the prebifurcation response; sources of this variability are discussed by Dunn et al. (2002). Although

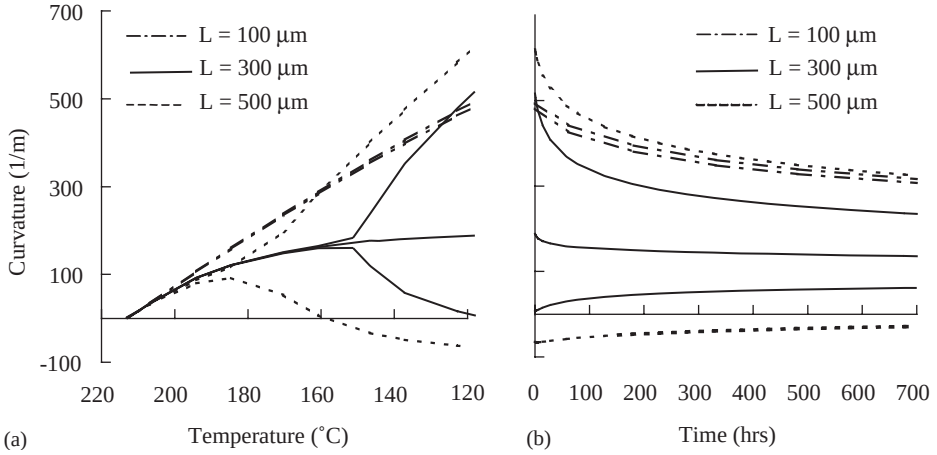

Fig. 11. Predicted curvature during cooling and during the isothermal hold at 120°C of $L \times 300$ μm gold (0.5 μm thick)/polysilicon (1.5 μm thick) plates with $L = 100$, 300, and 500 μm.

not shown, the predicted results show that as t increases further, the creep and stress relaxation will continue to unbuckle the plate to a circular mode. The initial increase in κ_y will be followed by a gradual decrease, along with the continuous decrease in κ_x with time. The rate that κ_x changes is greater than that of κ_y. The rate of decrease of curvature is very small after about half a year. A prediction shows that at the end of a 23 year isothermal hold, only about 15% of the initial $\kappa_x(88\ \mathrm{m}^{-1})$ remains and about 65% of the initial $\kappa_y(68\ \mathrm{m}^{-1})$ remains. The predictions qualitatively agree very well with the measurements. There are, however, quantitative discrepancies between the measurements and predictions, especially in the x direction. The predictions show slightly more rapid relaxation than the measurements. Nevertheless, the key phenomena are adequately predicted, including the interesting interaction between the material and structural nonlinearity.

In Fig. 11, we study the effect of the plate size and shape over a range of geometric parameters that is practically relevant for MEMS applications. The calculations were performed as previously described with $n = 5$ and $A = 5.2 \times 10^{-15}\ \mathrm{h}^{-1}\ \mathrm{MPa}^{-5}$, as inferred from the measurements in Fig. 8. Fig. 11a shows the average curvature vs. temperature during cooling for rectangular plates of size $L \times 300$ μm with $L = 100$, 300, and 500 μm. We have already discussed the behavior of the $L = 300$ μm plate, so here we will use it as a point of comparison for the other two plate shapes. For small temperature changes the curvature varies linearly with temperature change, but κ_x and κ_y depart from each other for the $L = 500$ μm plate after a temperature drop of only about 20°C. The deformation state then quickly approaches one of cylindrical bending as κ_x increases to about $600\ \mathrm{m}^{-1}$ at $T = 120$°C while κ_y decreases to about $-65\ \mathrm{m}^{-1}$. As mentioned before, with such large deformations the use of the average curvature as an accurate quantitative description of the deformation is questionable because the curvature varies considerably with position (see Freund, 2001; Dunn et al., 2002; and

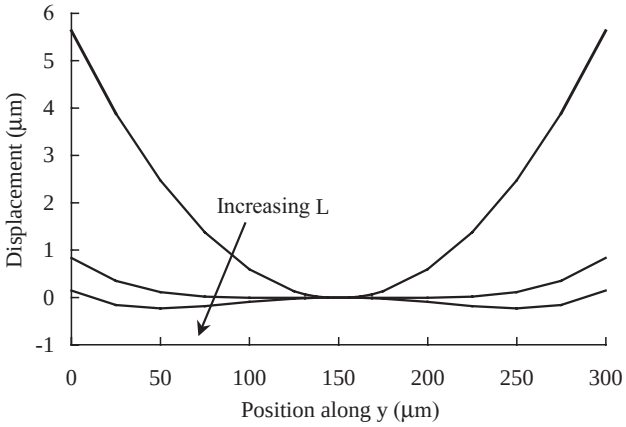

Fig. 12. Displacement profile along the y-axis for $L \times 300$ μm plates. The curves from top to bottom are for the $L = 100$, 300, and 500 μm structures, respectively.

also Fig. 12). The curvature of the $L = 100$ μm plate increases with the temperature change, and κ_x and κ_y depart from each other, but only slightly. The effect of geometric nonlinearity for this plate is small because of its relatively small size (as compared to the $L = 500$ μm plate). Our results regarding the plate size and shape are in agreement with the more comprehensive study of these effects by Finot and Suresh (1996). Fig. 11b shows the curvature evolution during the isothermal hold for these three plates. The behavior for the $L = 100$ μm plate consists of a gradual relaxation of both κ_x and κ_y to about 35 percent of their $t = 0$ value at $t = 700$ h. At $t = 700$ h, though, κ_x still differs slightly from κ_y due to the rectangular plate shape. The curvature evolution of the $L = 500$ μm plate is qualitatively similar to that of the $L = 300$ μm plate. Over time both κ_x and κ_y evolve significantly from their values at $t = 0$, however, at $t = 700$ h they are still quite different, indicating that the plate is still strongly deformed in an ellipsoidal mode.

In Fig. 12, we plot the computed displacement profile along the y direction for rectangular plates of size $L \times 300$ μm with $L = 100$, 300, and 500 μm after cooling to 120°C. For the $L = 100$ μm plate, the effect of the geometric nonlinearity is small as the deformation is nearly one of cylindrical bending. However this is not the case for the $L = 300$ and 500 μm plates. Upon cooling to 120°C, both plates bifurcated. Compared to the $L = 100$ μm plate, the magnitude of the displacement is small for the $L = 300$ and 500 μm plates, but the curvature varies significantly and even changes sign along the y-axis. The use of the average curvature is thus questionable. The average curvature over 150 μm region around the center of the plate (to be consistent with the 300 μm × 300 μm plate) is about $-65\ \mathrm{m}^{-1}$. The negative value means that the plate bends down, which is a misleading since the actual structure bends down around the center and then bends up near the edges. Averaging the curvature over the whole length, i.e., $L = 300$ μm, yields a value of $2.3\ \mathrm{m}^{-1}$. In the interest of simplicity we use the average curvature to describe the deformation, but remain aware of the variability in the curvature.

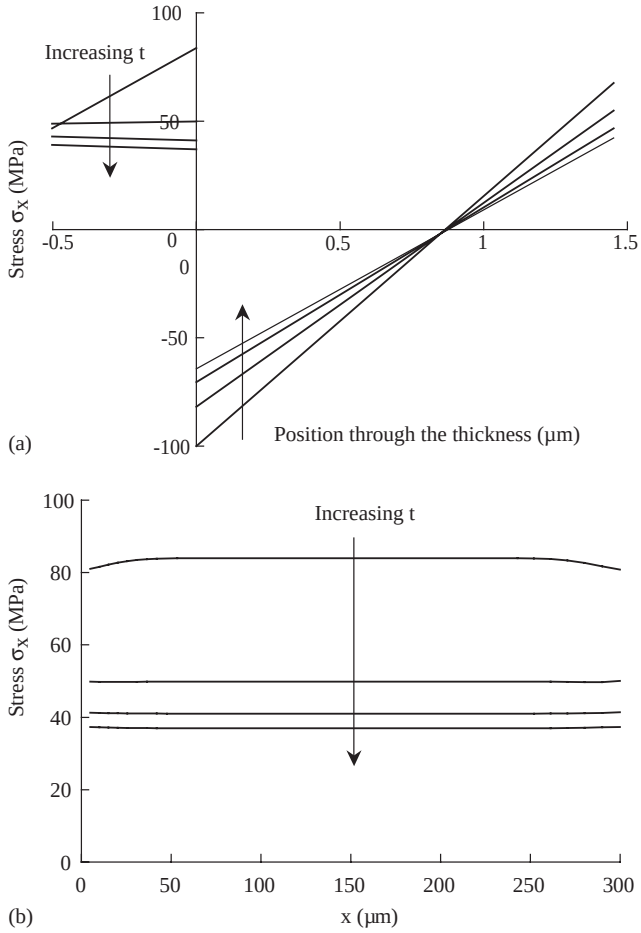

Fig. 13. Stress σ_x distribution for gold (0.5 μm thick)/polysilicon (1.5 μm thick) 300 μm × 50 μm beam during the stress relaxation process. (a) σ_x ($x = 150$ μm, $y = 0$) through the thickness. (b) σ_x along x ($y = 0$) at the interface of gold layer. Lines along the arrow direction correspond to $t = 0$, 160, 428, and 684 h, respectively.

Although not shown, we studied the effect of the power law constants A and n of the gold film on the curvature evolution during the isothermal hold. The results are qualitatively similar for beams and plates. Perhaps the most important observation is that the power law constant n can have a profound influence on the curvature evolution over the range typically reported for thin film metals. Changes in the constant A of two orders of magnitude are required to yield a quantitatively comparable effect on the curvature evolution. However, the effects of both A and n on the overall response are qualitatively similar, making it difficult to separate the two without further information.

In Figs. 13–15 we study the stress state in the beam and plates during the isothermal hold, as it drives the previously discussed curvature. Calculations are presented for the

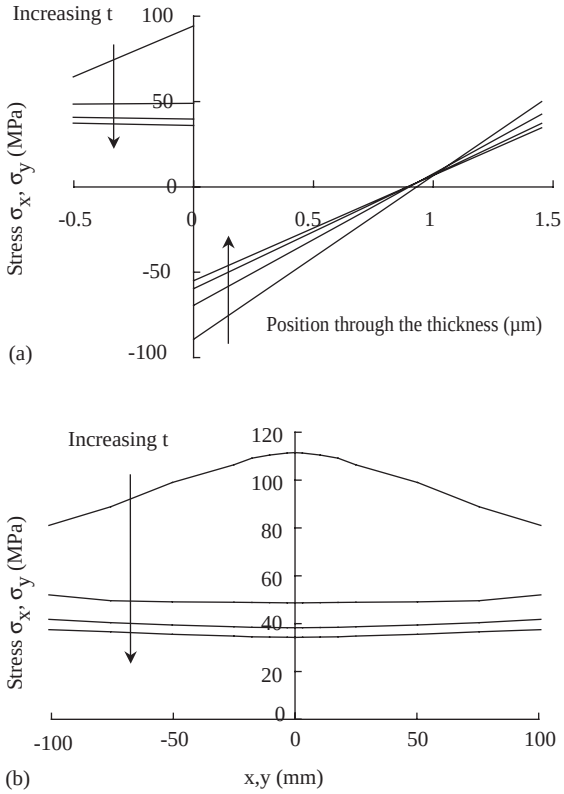

Fig. 14. Stress σ_x and σ_y distribution for gold (0.5 μm thick)/polysilicon (1.5 μm thick) 200 μm × 200 μm plate during the stress relaxation process. (a) σ_x ($x = 50$ μm, $y = 0$) and σ_y ($x = 0$, $y = 50$ μm) through the thickness. (b) σ_x along x ($y = 0$) and σ_y along y ($x = 0$) at the interface of gold layer. Lines along the arrow direction correspond to $t = 0$, 160, 428, and 684 h, respectively.

same times as used in Fig. 5; $t = 0$, 160, 428, and 684 h. In all cases the results are for the structures with a 0.5 μm gold film on a 1.5 μm thick polysilicon film. In Fig. 13 we show the evolution of the stress component σ_x through the thickness and along the length of a free beam. The stress in Fig. 13a is actually evaluated at a distance of 150 μm from the fixed end. As shown in Fig. 13b, the stress distribution along the length of the beam is essentially uniform. It is actually perturbed by the support post over about a 20 μm diameter region surrounding it. At $t = 0$ the stress state is thermoelastic and a significant stress gradient exists across both the gold and polysilicon films. As time increases the stress in the gold film relaxes due to the power-law creep. In order to satisfy overall equilibrium, the stress in the polysilicon film redistributes and decreases. The stress relaxes fastest at the region of highest stress, which due to the stress gradient, is at the interface. As a result, after only 160 h the stress gradient in the gold film is insignificant. Creep strains develop fastest at the interface and initially

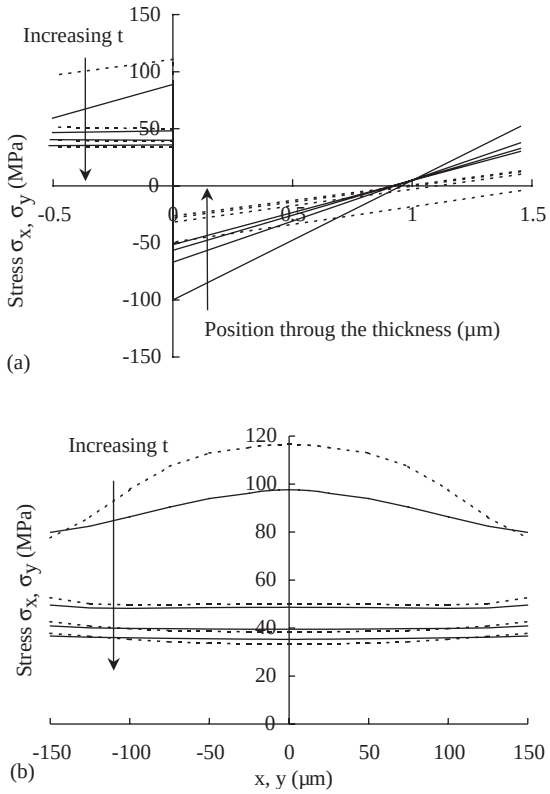

Fig. 15. Stress σ_x (solid lines) and σ_y (dotted lines) distribution for gold (0.5 μm thick)/polysilicon (1.5 μm thick) 300 μm × 300 μm plate during the stress relaxation process. (a) σ_x ($x = 75$ μm, $y = 0$) and σ_y ($x = 0$, $y = 75$ μm) through the thickness. (b) σ_x along x ($y = 0$) and σ_y along y ($x = 0$) at the interface of gold layer. Lines along the arrow direction correspond to $t = 0$, 160, 428, and 684 h, respectively.

vary nonlinearly through the thickness of the gold. After about 150 h, though, they are nearly linear through the gold with magnitudes that lead to the nearly constant stress distribution. More accurate continuum finite element calculations using a generalized plane strain formulation, which does not impose the thin-plate kinematics, confirm this. They also confirm that for the material and geometry parameters used here, the stress distribution is nearly linear through the thickness, even though the creep strains vary nonlinearly at short times. Although not shown, results for the beams with a 3.5 μm polysilicon film are similar, but the stress magnitude is higher in the gold and lower in the polysilicon. On the other hand, the stress gradient is less in both the polysilicon and the gold.

The through-thickness distribution of the biaxial stress $\sigma_x = \sigma_y$ at various times is shown in Fig. 14a for the $L = 200$ μm plate. The stress components shown are σ_x taken at $(x, y) = (50, 0)$ μm and σ_y taken at $(x, y) = (0, 50)$ μm. These are representative of the

average stress across the plate as seen in Fig. 14b. The behavior is similar qualitatively to that in Fig. 13a for the beam. Due to the geometric nonlinearity that occurs during cooling, the stresses are not uniform across the in-plane dimensions of the plate, unlike for the beam. This is shown in Fig. 14b where the stress components $\sigma_x\ (x, y = 0) = \sigma_y\ (x = 0, y)$ are shown at the four times. In addition to the significant stress gradient through the thickness, there exists an appreciable variation of the biaxial stress across the interface of the gold/polysilicon plate. This is consistent with observations of the spatial variation of the curvature (Freund et al., 1999; Freund, 2000; Finot et al., 1997; Lee et al., 2001; Dunn et al., 2002), and to a lesser degree the midplane strain (Dunn et al., 2002), that result from geometric nonlinearity. As with the through-thickness variation, the spatial variation in the x–y plane decreases significantly after only 160 h. Finally, in Fig. 15 we show analogous results for the $L = 300$ μm plate. The results for both the through-thickness and in-plane variations of the stress fields are similar to those for the $L = 200$ μm plates. The most significant difference is that because of the bifurcation, $\sigma_x \neq \sigma_y$. At $t = 0$, σ_y is about 20% higher than σ_x. As time increases, σ_x and σ_y converge. Like for the $L = 200$ μm plate, the stress gradient through the thickness also decreases to nearly zero, and the stress distribution across the in-plane dimensions becomes essentially uniform. While the calculations for both the $L = 200$ and 300 μm plates assume a free plate, other calculations considering the support post show that it perturbs the stress state over only about a 20 μm diameter region around the center.

6. Conclusions

We studied, both by experiments and modeling, the deformation of a series of micron-scale gold/polysilicon structures fabricated by a surface micromachining process and subjected to thermal loading. Both material and structural nonlinearity contributed to the observed response. The coupling of the two was apparent in plates where the initial cooling caused them to buckle, but the creep/stress relaxation then caused them to substantially unbuckle. We modeled the creep/stress relaxation process by assuming simple power-law creep in the gold, and assuming the polysilicon deformed elastically, but could not get fully self-consistent agreement between predictions and measurements. The use of a constant stress exponent $n = 5$ with a value of A that depends on the film thickness improved agreement substantially. The reasons for this are not completely clear, but are likely due to the neglect of a recovery mechanism in the gold film that opposes the creep/stress relaxation, and possibly a difference in creep deformation mechanisms. The results, though, do resonate with similar studies of thin films on thick substrates in microelectronics contexts. Finally, we carried out a parametric study of the effects of the structure shape and the power-law creep constants on the deformation, and studied the evolution of the stress state in the films both through the thickness and in the plane of the beams and plates. Initially a significant stress gradient exists through the thickness of the films, but over time the stresses became more uniform, and nearly constant in the creeping/relaxing film (gold), but the gradient remains in the elastic film (polysilicon).

Acknowledgements

This effort is sponsored by Sandia National Laboratories (Sandia/NSF Lifecycle Engineering Program) and the Air Force Office of Scientific Research (F49620-02-1-0037). We very much appreciate many beneficial discussions with Professor Ken Gall regarding deformation mechanisms in the gold film.

References

Baker, S.P., Kretschmann, A., Arzt, E., 2001. Thermomechanical behavior of different texture components in Cu thin films. Acta Mater. 49, 2145–2160.

De Groot, P., Deck, L., 1995. Surface Profiling by Analysis of White-Light Interferograms in the Special Frequency Domain. Journal of Modern Optics 42, 389–401.

Doerner, M.F., Nix, W.D., 1988. Stresses and deformation processes in thin-films on substrates. CRC Crit. Rev. Solid State and Mater. Sci. 14, 225–268.

Dunn, M.L., Zhang, Y., Bright, V., 2002. Deformation and structural stability of layered plate microstructures subjected to thermal loading. J. Microelectromech. Syst. 11, 372–384.

Fahnline, D.E., Masters, C.B., Salamon, N.J., 1991. Thin film stress from nonspherical substrate bending measurements. J. Vac. Sci. Technol. A 9, 2483–2487.

Finot, M., Suresh, S., 1996. Small and large deformation of thick and thin film multilayers: effects of layer geometry, plasticity and compositional gradients. J. Mech. Phys. Solids 44, 683–721.

Finot, M., Blech, I.A., Suresh, S., Fujimoto, H., 1997. Large deformation and geometric instability of substrates with thin film deposits. J. Appl. Phys. 81, 3457–3464.

Flinn, P.A., Gardner, D.S., Nix, W.D., 1987. Measurement and interpretation of stress in aluminum-based metallization as a function of thermal history. IEEE Trans. Electron Devices 34, 689–699.

Freund, L.B., 2000. Substrate curvature due to thin film mismatch strain in the nonlinear deformation range. J. Mech. Phys. Solids 48, 1159–1174.

Freund, L.B., Floro, J.A., Chason, E., 1999. Extension of the stoney formula for substrate curvature to configurations with thin substrate or large deformations. Appl. Phys. Lett. 74, 1987–1989.

Gall, K., West, N., Spark, K., Dunn, M.L., Finch, D., 2004. Creep of thin film Au on bimaterial Au/Si microcantilevers. Acta Mater. 52, 2133–2146.

Hershkovitz, M., Blech, I.A., Komem, Y., 1985. Stress-relaxation in thin aluminum films. Thin Solid Films 130, 87–93.

Huang, H., 1998. Mechanical properties of free-standing polycrystalline metallic thin films and multilayers. Ph.D. Thesis, Harvard University.

Hyer, M.W., 1981a. Some observations on the cured shape of thin unsymmetric laminates. J. Compos. Mater. 15, 175–194.

Hyer, M.W., 1981b. Calculation of the room-temperature shapes of unsymmetric laminates. J. Compos. Mater. 15, 296–310.

Hyer, M.W., 1982. The room-temperature shape of four-layer unsymmetric cross-ply laminates. J. Compos. Mater. 16, 318–340.

Keller, R.M., Baker, S.P., Arzt, E., 1999. Stress-temperature behavior of unpassivated thin copper films. Acta Mater. 47, 415–426.

King, J.A., 1988. Materials Handbook for Hybrid Microelectronics. Teledyne Microelectronics, Los Angeles, California.

Koester, D.A., Mahadevan, R., Hardy, B., Markus, K.W., 2001. MUMPs^{TM} Design Rules, Cronos Integrated Microsystems, A JDS Uniphase Company, http://www.memsrus.com/cronos/svcsrules.html

Koike, J., Utsunomiya, S., Shimoyama, Y., Maruyama, K., Oikawa, H., 1998. Thermal cycling fatigue and deformation mechanism in aluminum alloy thin films on silicon. J. Mater. Res. 13, 3256–3264.

Korhonen, M.A., Paszkiet, C.A., Black, R.D., Li, C.Y., 1990. Stress-relaxation of continuous film and narrow line metallizations of aluminum on silicon substrates. Scr. Metall. et Mater. 24, 2297–2302.

Laduzinsky, A.J., 2001. Stress relief for thin wafers. Design News, June 2001, pp. S9–S11.

Lee, H., Rosakis, A., Freund, L.B., 2001. Full-field optical measurement of curvatures in ultra-thin-film-substrate systems in the range of geometrically nonlinear deformations. J. Appl. Phys. 89, 6116–6129.

Legros, M., Hemker, K.J., Gouldstone, A., Suresh, S., Keller-Flaig, R.M., Arzt, E., 2002. Microstructural evolution in passivated Al films on Si substrates during thermal cycling. Acta Mater. 50, 3435–3452.

Leung, O.S., Munkholm, A., Brennan, S., Nix, W.D., 2000. A search for strain gradients in gold thin films on substrate using X-ray diffraction. J. Appl. Phys. 88, 1389–1396.

Masters, C.B., Salamon, N.J., 1993. Geometrically nonlinear stress-deflection relations for thin film/substrate systems. Int. J. Eng. Sci. 31, 915–925.

Masters, C.B., Salamon, N.J., 1994. Geometrically nonlinear stress-deflection relations for thin film/substrate systems with a finite element comparison. J. Appl. Mech. 61, 872–878.

Miller, D.C., Dunn, M.L., Bright, V.M., 2001. Thermally induced change in deformation of multimorph MEMS structures. In: Proc. SPIE International Symposium on Micromachining and Microfabrication—Reliability, Testing, and Characterization of MEMS/MOEMS, SPIE, Vol. 4558, pp. 32–44.

Nix, W.D., 1989. Mechanical properties of thin films. Metall. Trans. A 20A, 2217–2245.

Salamon, N.J., Masters, C.B., 1995. Bifurcation in isotropic thin film/substrate plates. Int. J. Solids Structures 32, 473–481.

Sharpe, W.N., 2002. Mechanical properties of MEMS materials. A chapter in the MEMS Handbook. M. Gad-el-Hak ed., CRS Press.

Shen, Y.L., Suresh, S., 1995. Thermal cycling and stress relaxation response of Si–Al and Si–Al–SiO_2 layered thin films. Acta Metall. Mater. 43, 3915–3926.

Shute, C.J., Cohen, J.B., 1992. Stress-relaxation in Al–Cu thin-films. Mater. Sci. Eng. A-Structural Materials Properties Microstructure and Processing 149, 167–172.

Spolenak, R., Brown, W.L., Tamura, N., MacDowell, A.A., Celestre, R.S., Padmore, H.A., Valek, B., Bravman, J.C., Marieb, T., Fujimoto, H., Batterman, B.W., Patel, J.R., 2003. Local plasticity of Al thin films as revealed by X-ray microdiffraction. Phys. Rev. Lett. 90, Art. No. 096102.

Stoney, G.G., 1909. The tension of metallic films deposited by electrolysis. Proc. Roy. Soc. London A 82, 172–175.

Thouless, M.D., 1995. Modeling the development and relaxation of stresses in films. Annu. Rev. Mater. Sci. 25, 69–96.

Thouless, M.D., Cupta, J., Harper, J.M.E., 1993. Stress development and relaxation in copper films during thermal cycling. J. Mater. Res. 8, 1845–1852.

Thouless, M.D., Rodbell, K.P., Cabral, C., 1996. Effect of a surface layer on the stress relaxation of thin films. J. Vac. Sci. Technol. A 14, 2454–2461.

Vickers-Kirby, D.J., Kubena, R.L., Stratton, F.P., Joyce, R.J., Chang, D.T., Kim, J., 2001. Anelastic creep phenomena in thin film metal plated cantilevers for MEMS. In: Mater. Res. DSoc. Symp., Vol. 657, pp. EE2.5.1–EE2.5.6.

Vinci, R.P., Zielinskiem, E.M., Bravman, J.C., 1995. Thermal strain and stress in copper thin-films. Thin Solid Films 262, 142–153.

Weiss, D., Gao, H., Arzt, E., 2001. Constrained diffusional creep in UHv-produced copper thin films. Acta Mater. 49, 2395–2403.

Zhang, Y., Dunn, M.L., 2003. Deformation of blanketed and patterned bilayer thin film microstructures during post-release and cyclic thermal loading. J. Microelectromech. Syst. 12, 788–796.